engineering proceedings

MDPI

Proceeding Paper

Design of a Light-Weight Vertical Tail for a Hybrid High-Altitude Pseudo-Satellite †

Feliciano Di Biase *, Domenico Varricchio, Vincenzo Rosario Baraniello and Giuseppe Persechino

Italian Aerospace Research Centre, Via Maiorise snc, 81043 Capua, Italy; d.varricchio@cira.it (D.V.); v.baraniello@cira.it (V.R.B.); g.persechino@cira.it (G.P.)

* Correspondence: f.dibiase@cira.it

† Presented at the 14th EASN International Conference on "Innovation in Aviation & Space towards sustainability today & tomorrow", Thessaloniki, Greece, 8–11 October 2024.

Abstract: The interest in high-altitude pseudo-satellites (HAPSs) has significantly increased in recent years due to the great versatility of these platforms, which allows them to be employed in a wide variety of applications in civilian and military fields. This study focuses on the design of an innovative hybrid airship vertical tail. The empennage proposed is internally sustained with a light-weight structure and coated with a thin film, avoiding any leakage that would occur with inflated structural elements. The design of the vertical tail and its structural analysis through a detailed finite element (FE) model are presented to show its overall behavior subjected to the aerodynamic loads.

Keywords: HAPS; stratospheric platform; vertical tail HAPS; light-weight structure; structural design; aerospace fabric structure; FE model; finite element analysis

check for updates

Academic Editors: Spiros Pantelakis, Andreas Strohmayer and Nikolaos Michailidis

Published: 11 March 2025

Citation: Di Biase, F.; Varricchio, D.; Baraniello, V.R.; Persechino, G. Design of a Light-Weight Vertical Tail for a Hybrid High-Altitude Pseudo-Satellite. *Eng. Proc.* **2025**, *90*, 19. https://doi.org/10.3390/engproc2025090019

Copyright: © 2025 by the authors. Licensee MDPI, Basel, Switzerland. This article is an open access article distributed under the terms and conditions of the Creative Commons Attribution (CC BY) license (https://creativecommons.org/licenses/by/4.0/).

1. Introduction

HAPSs have seen a remarkable increase in recent decades as a valid complementary solution to satellites and RPASs (Remotely Piloted Aerial Systems) [1]. These types of structures can include free-floating balloons, airships, or powered fixed-wing aircrafts that use either solar power or an on-board energy source. High-altitude pseudo-satellites are employed in a wide variety of applications in civilian and military fields, such as for improvements in telecommunications, astronomy, emergency applications, remote sensing, scientific explorations, cargo transportation, observation, and surveillance [2,3]. Typically, these platforms fly at an altitude of about 18–20 km, which is characterized by weak winds and the absence of meteorological phenomena [4,5]. These conditions facilitate mission operations. The aim of this paper is to describe the design process of a vertical tail (VT) for a hybrid airship. This type of vehicles can generate aerodynamic forces like a fixed-wing and aerostatic ones like balloons and airships [6,7]. An example of a hybrid platform is shown in Figure 1. Taking part in the lateral–directional stability of the platform, the design of the tail assembly is essential to guarantee safety during flight. Indeed, the lateral–directional degree of freedom are strictly coupled. The tail provides the main contribution to the directional stability. When the side-slip angle is not equal to zero, it generates a force and, thus, a yaw moment, which restores the attitude of the platform. This tendency is named positive weathercock stability [8–10]. The design process is carried out pursuing the right compromise among multiple constraints of different nature, with the aim of achieving a solution that weighed as low as possible because a low structural weight allows the mass of the entire airship to be contained. Moreover, this implies the following: (1) less material is needed to create the different parts that make up the platform; (2) and there is

reduced energy consumption for flight, consequently limiting the environmental impact and economic expenses.



Figure 1. Example of a hybrid airship.

2. Materials and Methods

2.1. Design Process

The proposed tail empennage is characterized by a dihedral angle close to 90°, allowing us to treat it, for all intents and purposes, as a vertical aerodynamic surface. The design process begins with the evaluation of the vertical tail volume coefficient C_{VT}. This parameter concerns the hybrid airship volume, center of gravity, and length to the tail surface, particularly in the following:

$$C_{VT} = \frac{l_{VT} \cdot S_{VT}}{l_b \cdot Vol^{2/3}} \quad (1)$$

where l_{VT} is the distance between the center of gravity of the platform and the quarter chord of the VT mean aerodynamic chord; l_b is the airship body length; S_{VT} is the previously mentioned tail surface; and Vol is the platform volume. A considerable amount of C_{VT} values, as a function of volume platforms, can be found in [9]. Interpolating these values, the VT volume coefficient is obtained as described in [9]. At this stage, S_{VT} can be calculated by imposing a reasonable assumption for the position of the vertical tail aerodynamic center, which is not fully defined. The planform vertical tail area is then employed to estimate the weight of vertical empennage and to define an updated value of the center of gravity, knowing the weight of all the remaining platform structures. During the preliminary design phase, a prediction of the mass value of the light-weight vertical tail can be obtained as follows [9]:

$$W_{VT} = F_{PSQ} \cdot S_{VT} \cdot F_{AF} \quad (2)$$

where F_{AF} takes into account the tail external attach fittings, and F_{PSQ} is the surface density (kg/m^2) used to fabricate the tail surface out of light-weight structural materials. As shown in Figure 2, the process is iterative. Finally, the area and layout of the tail are refined through aerodynamic, flight mechanics and stability/control analyses. The forward step is the CAD/CAE design phase, based on the restrictions reported in the "Constraints" block of Figure 2 and the results of the FE analysis. The structural design loads, applied to the finite element model, are derived from the subpart C-structure of JARUS CS-LUAS considering the flight profile of the platform. The choice falls on these recommendations because, at the moment of writing, the specific regulation for HAPS is not yet well-assessed. A safety factor of 1.5 is imposed to the limit loads, as specified in CS-LUAS 303, while the sections considered to evaluate the loads under different flight conditions are CS-LUAS 441 and CS-LUAS 443 [11]. This phase is also characterized by an iterative procedure.

In Table 1, the geometrical features of the aerodynamic surface are listed. The vertical empennage is characterized by a symmetrical airfoil which responds in a symmetric manner to positive and negative side-slip angles.

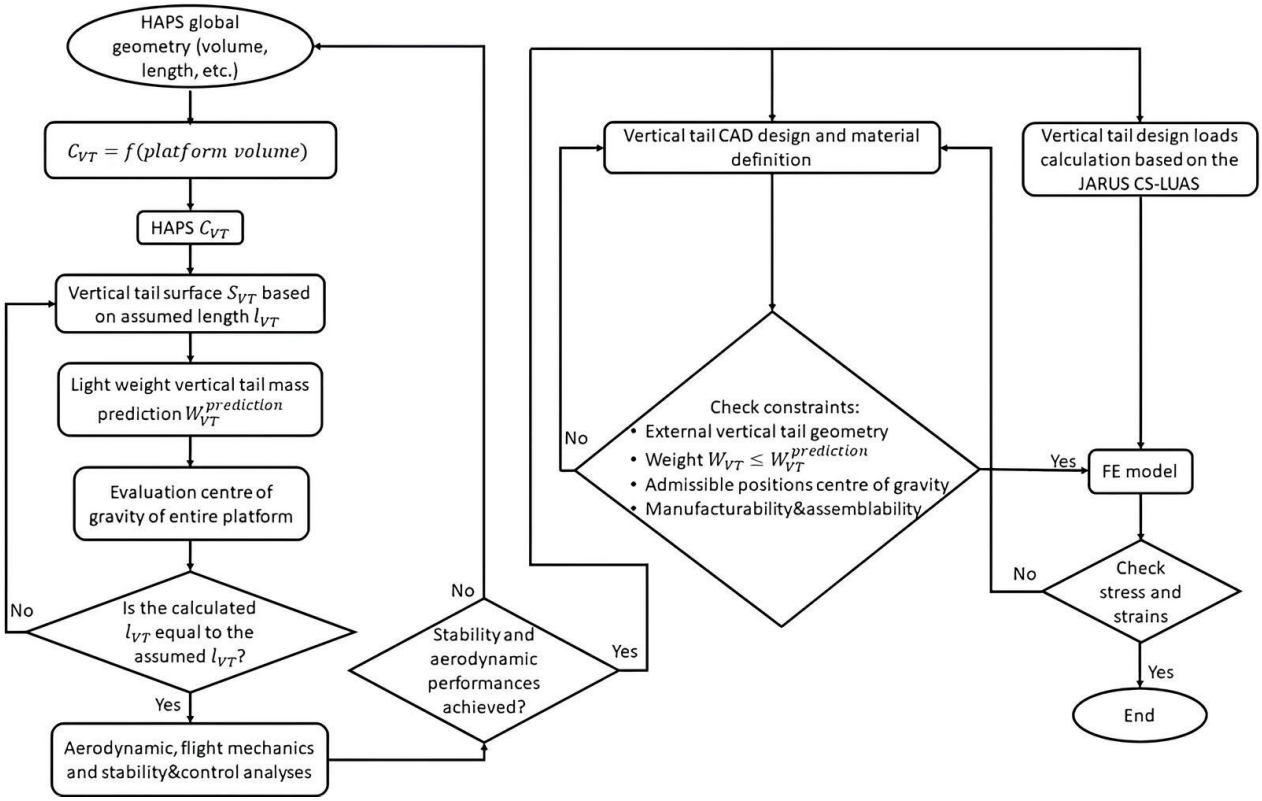


Figure 2. Design workflow.

Table 1. Geometrical parameters of the vertical tail.

Geometrical Parameter	Value
Geometric mean chord	1.3 [m]
Dihedral angle Γ	75.0°
VT swept angle Λ_{LE} / Wing swept angle Λ_{LE}	1.2

2.2. CAD Model

In Figure 3, the CAD model, representative of the vertical tail, is shown. The employed software is Autodesk Fusion 2024.

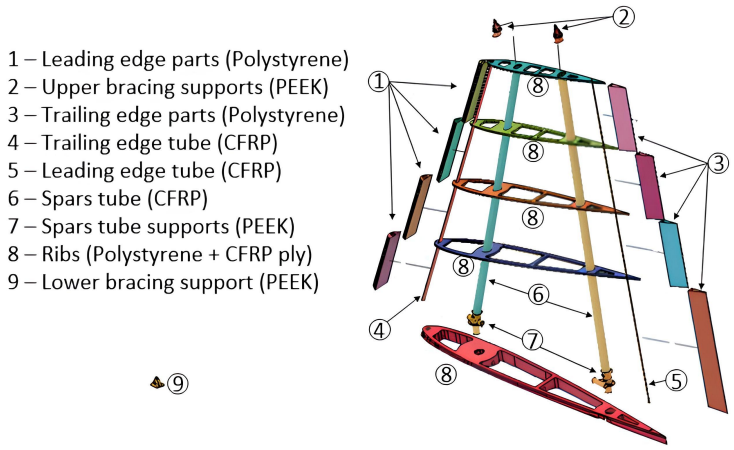


Figure 3. Vertical tail CAD model.

A configuration with a light-weight structure and coated with a thin film was preferred over an inflated one. Generally, the latter is pressurized like the envelope, requiring a heavier fabric skin to avoid leakage, thus with a more sophisticated manufacturing technique and additional weight increase. The used material for the different components is indicated between the brackets in Figure 3. The external skin, made of fabric material, has the function of containing the internal structure and transmitting the aerodynamic forces to the ribs. The chosen material is subjected to mechanical and thermal stress, deteriorating actions of external agents such as ultraviolet rays and ozone. Clearly, no single material is capable of offering all the desired characteristics; consequently, multi-layer one is adopted, in which each layer performs a certain function [12]. The inner structure of the vertical tail features two circular carbon fiber tubes that act as empennage spars, which ensure the desired high torsional rigidity, maintaining the weight to be as low as possible. The arrangement of these tubes is dictated by the necessity to support aerodynamic loads, conventionally applied to a quarter chord. The ribs, sustained by the spars, have the aim to maintain the external shape of the tail. Furthermore, a carbon fiber tube is inserted in the LE and TE to support them. The above-mentioned parts are bonded together with an epoxy resin, giving the required compactness. The spars are constrained to the platform structure by means of polyether ether ketone (PEEK) supports and connected together by means of screws, allowing for the fitting, the replacement, and the removal of VT in the event of damage. Two dyneema cables connect the lower bracing support with the bracing upper supports (which are glued to the spars). This link is crucial to prevent excessive deformation of the aerodynamic surface, resulting in a loss of efficiency. The Young modulus of dyneema is obtained following the hypothesis of linear elastic material and the data provided by the manufacturer. In Table 2, the characteristics of the adopted materials are shown [13–15].

Table 2. Material properties.

Material	Young Module E_l [MPa]	Young Module E_t [MPa]	Poisson's Ratio ν	Density ρ [kg/m^3]
Prepreg	163,000.0	12,000.0	0.28	1570.0
PEEK	3600.0	-	0.35	1320.0
Polystyrene	3200.0	-	0.35	1021.0
Dyneema	44,000.0	-	-	970.0

2.3. FE Model

An FE model of the vertical tail, based on the previous CAD model, is created to investigate the mechanical behavior. The used software for the pre- and post-processing phases is Simcenter FEMAP 2306. MSC Nastran 2024.1 is employed as solver. Considering their shape, the spars, the external plies of ribs, and the LE and TE tubes are discretized through quadrilateral 2D linear shell elements. A laminate structure is adopted to represent the orthotropic composite material they are made of. In particular, three different properties are created, considering the thickness of plies that characterize these parts. The spar tube supports, the core of ribs, the polystyrene LE/TE parts, and the bracing supports are meshed with parabolic tetrahedral elements, comprising an elastic linear isotropic material. To simulate the bonding between the different parts of the vertical tail, connectors based on glue contact type are implemented in the FE model. This contact type blocks relative displacements between the involved surfaces, allowing the interaction between multiple bodies. The dyneema cable is modeled using rod-type elements with an associated axial

stiffness. The direction and the verse of the aerodynamic load only induces tension in the bracing. The assigned value to the stiffness is the result of the expression.

$$K_{rod} = \frac{E \cdot A}{L} \tag{3}$$

in which A and L represent the cable section and length, respectively. The cable section is chosen to avoid failures. The lower bracing support and the spar tube supports are constrained in all six degrees of freedom (DOFs). According to the JARUS CS-LUAS regulations, the aerodynamic load L is expressed as follows:

$$\begin{aligned} L = \frac{1}{2}\rho V_{fin}^2(\cos^2\beta\cos^2\alpha + \sin^2\beta\sin^2\Gamma + \cos^2\beta\sin^2\alpha\cos^2\Gamma \pm \\ 2\sin\beta\cos\beta\sin\alpha\cos\Gamma\sin\Gamma)S_{VT} \cdot C_{l_\alpha}[\arctan\left(\frac{\tan\beta\sin\Gamma}{\cos\alpha} \pm \tan\alpha\cos\Gamma\right)]_{rad} \end{aligned} \tag{4}$$

where ρ is the air density, V_{fin} is the air velocity impacting the vertical tail, and C_{l_α} is the lift coefficient gradient. The sign $\pm$ is related to the vertical tail under consideration, i.e., the right or the left empennage. L, acts orthogonally to the vertical tail planform area, and it is the result of the flight conditions, characterized by an angle of attack α and a side-slip angle β. Depending on the values of α, β, the approximation $\sin x \simeq x_{rad}$, $\cos x \simeq 1$ can be adopted. An expression of C_{l_α} that is consistent with CFD analysis is expressed as follows [16]:

$$C_{l_\alpha} = \frac{\pi}{2}AR \quad [\frac{1}{rad}] \tag{5}$$

The Equation (5) is reasonable for an aspect ratio AR smaller than 1.5. The vector load in Equation (4) must be added with the lateral gust F_g, which is defined as follows:

$$F_g = \frac{1}{2}\rho V_{fin}S_{VT}\frac{\pi}{2}AR \cdot K \cdot U_{de}\sin^2\Gamma \tag{6}$$

where the projection of empennage in the vertical aircraft plane of symmetry $x_B - z_B$ is considered. U_{de} is the intensity of lateral gust, while K is the attenuation gust factor, with a definition that can be found in [11]. A series of load cases are derived according to the regulations; consequently, the loads in Equations (4) and (6) are calculated. The worst-case scenario, in terms of loads, is examined to understand the size of the internal structures of the empennage. It is worth noting that, in the analyzed configuration, the loads, due to the projection of empennage in the horizontal aircraft plane $x_B - y_B$, are negligible compared to those of the vertical projection because of the high value of angle Γ. For structural purposes, the load (4) and (6) must be distributed over the vertical tail area and vector-summed in the directions orthogonal and parallel to the empennage planform area. The lift per unit span is assumed to be located at one quarter chord, and the intensity can be derived by means of the Schrenk method [17,18] which is a semi-graphical approach to calculate cC_l, with c and C_l, which represent the chord and the section lift coefficient, respectively. Then, this parameter is adjusted to take into account the effect of dihedral and swept angles. Therefore, the lift-section distribution is written as follows:

$$L'_{Schrenk} = \frac{1}{2}\rho V_{fin}^2[c\,C_l]_\Lambda\cos\Gamma \tag{7}$$

where $[c\,C_l]_\Lambda$ represents the lift distribution considering the swept angle. The regulations specify how to distribute gust $L'_g(\frac{x}{c})$ along the chord (Figure 4).

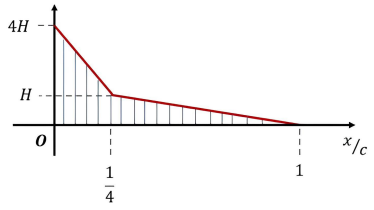


Figure 4. $L'_g(\frac{x}{c})$ distribution along the chord.

The parameter H is derived by imposing the value of F_g calculated through Equation (6). It is easy to demonstrate that the point of application of $L'_g(\frac{x}{c})$ is at the quarter chord, and the gust distribution along the span F'_g is expressed as follows:

$$F'_g = Hc \tag{8}$$

where c is a function that describes the variation in the chord along the span of the empennage. The span-wise distributions in the orthogonal and parallel directions to the planform vertical tail area are expressed as follows:

$$F'_\perp = L'_{Schrenk} + F'_g \sin\Gamma \tag{9}$$

$$F'_\parallel = F'_g \cos\Gamma \tag{10}$$

In the treated case study, $F'_\parallel$ is negligible compared to $F'_\perp$. Figure 5 shows the non-dimensional orthogonal force, increased by a factor of 1.5, compared to the non-dimensional span-wise direction. The dimensionless factor includes the maximum values.

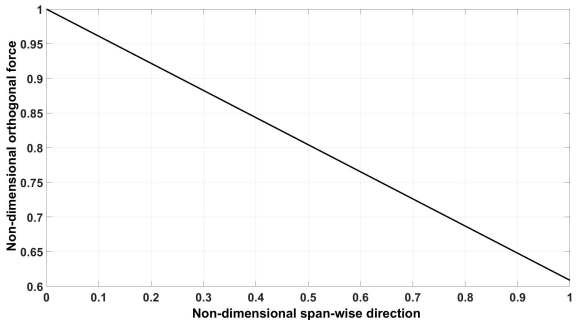


Figure 5. $F'_\perp$ distribution along the span-wise direction.

The distribution, applied at one-quarter of the chord, is redistributed on each rib and, through RBe3 elements, divided among the elements of the lateral surfaces of the ribs. This way, the load is transmitted to the spars. The load acting on each rib is derived from the following equation:

$$P_{rib} = \int_{z_i}^{z_{i+1}} F'_\perp \, dz \tag{11}$$

where i goes from 0 to 4, and z is the coordinate along the span-wise direction of the vertical tail. z_1 and z_4 represent the coordinates of the root and tip ribs, while the other z_i describes the coordinate of the middle point between two consecutive ribs. Figure 6 shows the non-dimensional values of the applied forces, dimensionless with respect to the maximum value.

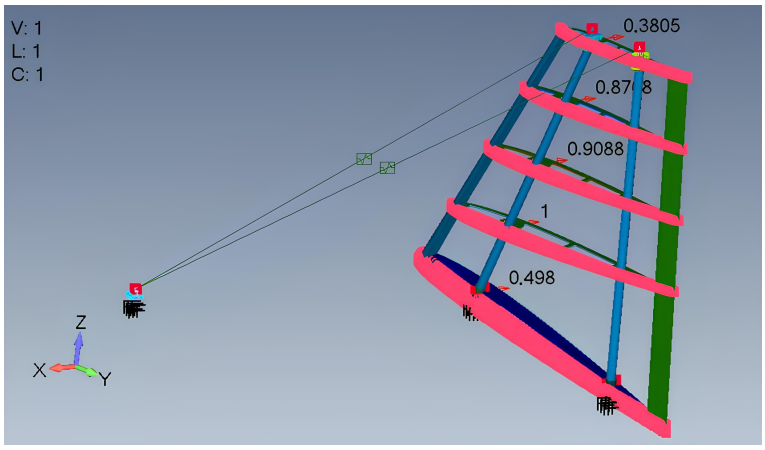


Figure 6. FE Model.

3. Results and Discussion

Figure 7A shows the maximum displacement of the vertical tail with the adoption of the bracing. This permits the reduction in the effect of the gust load, as seen in Figure 7B, in which the bracing cables are absent. Indeed, in the latter case, the maximum displacement is 21.39 mm instead of 3.85 mm. Furthermore, there is also a variation in the trend of displacement along the span-wise direction. Figure 7C reports the maximum stress (23.73 MPa) calculated with the von Mises yield criterion. This value is reached in the bracing upper support. For the chosen material, the yielding strength is equal to 70 MPa. Consequently, the safety factor is $\simeq$2.95. Due to the nature of the CFRP laminate, the adoption of a failure criterion is necessary. Among the available options, the Tsai–Wu criterion is selected, as it can describe complex failure modes under both tension and compression, providing a more accurate prediction of failure behavior under combined loading conditions [19]. The criterion indicates that the material will not fail if the following expression is fulfilled:

$$F_1\sigma_1 + F_2\sigma_2 + F_{11}\sigma_1^2 + F_{22}\sigma_2^2 + 2F_{12}\sigma_1\sigma_2 + F_6\tau_{12} + F_{66}\tau_{12}^2 \leq 1 \quad (12)$$

In Figure 7D, the laminate failure index is illustrated; the maximum value is reached in the front spar, at the location where it connects to the support.

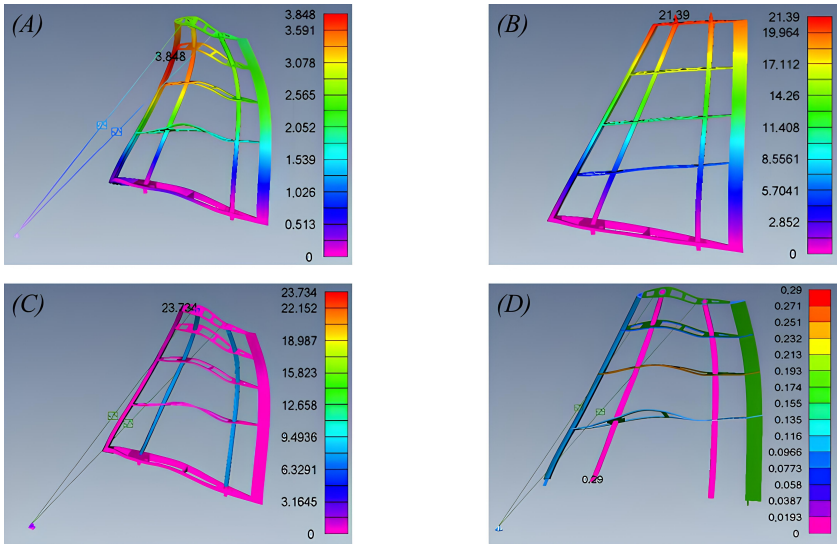


Figure 7. FE Results: (**A**) total displacement with bracing [mm]; (**B**) total displacement without bracing [mm]; (**C**) von Mises stress [MPa]; (**D**) Tsai–Wu laminate failure index.

Finally, the weights of the innovative structure and of the light-weight classical structure is calculated and compared.

Table 3 highlights that the proposed structure results in a saving of almost 70% of the predicted weight.

Table 3. Weight comparison.

Structure	Weight [kg]
Light-weight classical	3.47
Innovative proposed	1.10

4. Conclusions

This work presents the design of a vertical tail for a hybrid airship. The aim is to provide guidelines for the design of structures based on parts made of materials such as polystyrene, fabrics, and thermoplastics that can be of great interest for the HAPS. The FE analysis results show that the designed structure can withstand external loads without compromising the shape and the aerodynamic efficiency of the vertical tail. The selected materials and the arrangement of various components enabled the design to meet the constraints that guided the design process. The weight reduction in the vertical tail impacts the overall design of the hybrid airship structure, enabling the reduction in the maximum take-off weight (MTOW). This is in accordance with the environmental sustainability policies that the aviation field is heading towards. The next steps will be the manufacturing phase of the described assembly and the testing of it. The acquired data will be used to validate the FE model, comparing the numerical results with experimental measurements.

Author Contributions: Conceptualization, V.R.B. and G.P.; methodology, F.D.B. and D.V.; software, F.D.B. and D.V.; validation, D.V.; formal analysis, F.D.B.; writing—original draft preparation, F.D.B. and D.V.; writing—review and editing, V.R.B. and G.P.; visualization, F.D.B.; supervision, V.R.B. and G.P. All authors have read and agreed to the published version of the manuscript.

Funding: This research received no external funding.

Institutional Review Board Statement: Not applicable.

Informed Consent Statement: Not applicable.

Data Availability Statement: The datasets presented in this article are not readily available because the data are part of an ongoing study. Requests to access the datasets should be directed to corresponding author.

Conflicts of Interest: The authors declare no conflicts of interest.

References

1. Baraniello, V.R.; Persechino, G.; Borsa, R. Tools for the Conceptual Design of a Stratospheric Hybrid Platform. In *SAE Technical Paper*; No. 2020-01-0025; SAE International: Warrendale, PA, USA, 2020.
2. Araripe d'Oliveira, F.; Cristovão Lourenço de Melo, F.; Campos Devezas, T. High-altitude platforms—Present situation and technology trends. *J. Aerosp. Technol. Manag.* **2016**, *8*, 249–262. [CrossRef]
3. Gonzalo, J.; Lopez, D.; Dominguez, D.; García, A.; Escapa, A.; Borsa, R. On the capabilities and limitations of high altitude pseudo-satellites. *Prog. Aerosp. Sci.* **2018**, *98*, 37–56. [CrossRef]
4. Sinko, J. High altitude powered platform—A microwave powered airship. In Proceedings of the 3rd Lighter-Than-Air Systems Technology Conference, American Institute of Aeronautics and Astronautics, Palo Alto, CA, USA, 11–13 July 1979.
5. De Grado, J.G.; Tascon, C.S. On the development of a digital meteorological model for simulating future air traffic management automation. In Proceedings of the 2011 20th IEEE International Workshops on Enabling Technologies: Infrastructure for Collaborative Enterprises Art,Paris, France, 27–29 June 2011; pp. 223–228.
6. Khoury, G.A. *Airship Technology*, 2nd ed.; Cambridge University Press: New York, NY, USA, 2012; p. 5

7. ul Haque, A.; Asrar, W.; Sulaeman, E.; Omar, A.; Ali, J.S.M. Pugh Analysis for Configuration Selection of a Hybrid Buoyant Aircraft. Technical Report. In *SAE Technical Paper*; SAE International: Warrendale, PA, USA, 2015. [CrossRef]
8. Gudmundsson, S. Requirements for Static Directional Stability, In *General Aviation Aircraft Design: Applied Methods and Procedures*; Elsevier: Amsterdam, The Netherlands; Publishing House: Oxford, UK, 2014; pp. 460, 476–477.
9. Grant Carichner, E.; Leland Nicolai, M. Subsystems and Weights, In *Fundamentals of Aircraft and Airship Design, Volume II—Airship Design and Case Studies*; American Institute of Aeronautics and Astronautics, Inc.: Reston, VA, USA, 2013; Chapters 7, 9, 10.
10. Etkin, B.; Reid, L.D. *Dynamics of Flight: Stability and Control*; John Wiley & Sons: Hoboken, NJ, USA, 1995; pp. 79–93.
11. Farner, M. JARUS CS-LUAS. Recommendations for Certification Specification for Light Unmanned Aeroplane Systems; JAR_DEL_WG3_D.04. Available online: http://jarus-rpas.org/wp-content/uploads/2023/06/jar_07_doc_CS_LUAS.pdf (accessed on 2 September 2024).
12. Zhai, H.; Euler, A. Material challenges for lighter-than-air systems in high altitude applications. In Proceedings of the AIAA 5th Aviation, Technology, Integration, and Operations Conference, Arlington, VA, USA, 27 September 2005.
13. Hexcel Corporation. Prepreg Data Sheet. HexPly 8552. Available online: https://www.hexcel.com/user_area/content_media/raw/HexPly_8552_eu_DataSheet(1).pdf (accessed on 2 September 2024).
14. Matweb. Overview of Materials for Polyetheretherketone. Unreinforced. Available online: https://www.matweb.com/search/datasheet_print.aspxmatguid=2164cacabcde4391a596640d553b2ebe (accessed on 2 September 2024).
15. Matweb. Overview of Materials for Polystyrene, Molded. Unreinforced. Available online: https://www.matweb.com/search/datasheettext.aspx?matguid=48055b1b098041ba8e8eb06c64064e93 (accessed on 2 September 2024).
16. Obert, E. *Aerodynamic Design of Transport Aircraft*; IOS Press: Amsterdam, The Netherlands, 2009; pp. 413–422
17. Oskar, S. A simple approximation method for obtaining the spanwise lift distribution. *Aeronaut. J.* **1941**, *45*, 331–336.
18. Kamal, N.N.M.; Basri, A.A.; Basri, E.I.; Basri, I.S.; Abas, M.F. Comparison study between Schrenk's approximation method and computational fluid dynamics of aerodynamic loading on UAV NACA 4415 wing. *J. Adv. Res. Fluid Mech. Therm. Sci.* **2019**, *64*, 283–292.
19. Tsai, S.W.; Wu, E.M. A General Theory of Strength for Anisotropic Materials. *J. Compos. Mater.* **1971**, *5*, 58–80. [CrossRef]

Disclaimer/Publisher's Note: The statements, opinions and data contained in all publications are solely those of the individual author(s) and contributor(s) and not of MDPI and/or the editor(s). MDPI and/or the editor(s) disclaim responsibility for any injury to people or property resulting from any ideas, methods, instructions or products referred to in the content.